Available online at www.sciencedirect.com
SCIENCE DIRECT
Chemical Physics Letters 426 (2006) 351–356
CHEMICAL PHYSICS LETTERS
www.elsevier.com/locate/cplett

Characterization of $C^+_{n=2-16}$ clusters produced by electronic sputtering

Franciso Alberto Fernandez-Lima [a,b], Cassia Ribeiro Ponciano [a], Enio Frota da Silveira [a], Marco Antonio Chaer Nascimento [c,*]

[a] Physics Department, Pontifícia Universidade Católica, Rua Marques de São Vicente 225, C.P. 38071, Rio de Janeiro 22543-970, Brazil
[b] Instituto Superior de Tecnologías y Ciencias Aplicadas, Ave Salvador Allende esq. Luaces, sln, AP 6163, CP 10600, Ciudad de La Habana, Cuba
[c] Instituto de Química, Universidade Federal do Rio de Janeiro, Cidade Universitária, CT Bloco A sala 412, Rio de Janeiro 21949-900, Brazil

Received 10 April 2006; in final form 10 May 2006
Available online 20 May 2006

Abstract

The structures and abundances of $C^+_{n=2-16}$ clusters produced by electronic sputtering from the impact of ^{252}Cf fission fragments on CO ice and from the UV laser desorption of amorphous carbon and graphite targets are analyzed. A systematic search for the more stable conformers at the DFT/B3LYP level of calculation and their contribution to the mass spectra is reported. A new methodology for a proper taxonomic description of the cluster isomers is proposed. Besides the known linear and monocyclic clusters series, new members of these series and two new series are described: the bi-cyclic and/or tri-cyclic and the rhombic core series.

1. Introduction

The study of pure carbon molecules has attracted great astrophysical interest since they have been identified in the atmospheres of carbon stars, comet tails and interstellar molecular clouds. In addition, the knowledge of the physical and chemical properties of carbon clusters is important for understanding a large variety of chemical systems such as: hydrocarbon flames, soot-forming, thin diamond and silicon carbide films and nanotubes production.

The vast literature about carbon clusters prior to year 2000 can be found in the extensive review articles [1–3]. Briefly, carbon clusters have been produced by a variety of methods (e.g. laser vaporization, electron impact, ion bombardment and sparks) and from a number of systems (e.g. graphite, synthetic diamond, glassy carbon, carbon nanotubes, diamond like films, condensed gases and organic polymers) [4–12]. For small carbon clusters ($n < 20$), it is remarkable the relative high abundances of the C^+_n, $n = 3$, 5, 7, 11, 15 and 19 species in the mass spectra of laser vaporization experiments from graphite targets [8,9]. For clusters produced by ion bombardment of organic polymers and by sparks, an odd/even periodicity of C^+_n intensities was observed [10,11]. The structures of small ionic carbon clusters have been indirectly determined by ion chromatography [13,14].

On the theoretical side, small neutral carbon clusters were studied at the semi empirical MO [15], *ab initio* (Hartree Fock, Moller Plesset perturbation theory) and density functional theory (DFT) levels [2,16–24]. However, just a few calculations have been reported for positively charged carbon clusters. Most of the studies of the C^+_n ($n = 1$–10) ions were focused on the description of their structures [2,19,24] and, as a general result, only linear and cyclic structures were found.

In the present work, the distributions of carbon clusters produced by electronic sputtering from three different targets are analyzed. The C^+_n clusters were obtained by the impact of ^{252}Cf fission fragments (FF) on CO ice and by 337 nm UV laser desorption of amorphous carbon and of graphite targets. A systematic search for the more stable geometries at the DFT/B3LYP/6-311G** level of calculation is presented and their contribution to the mass spectra intensities is discussed. The carbon cluster production/ionization mechanisms are also discussed.

* Corresponding author. Fax: 55 21 25627265.
E-mail address: chaer@iq.ufrj.br (M.A.C. Nascimento).

0009-2614/$ - see front matter © 2006 Elsevier B.V. All rights reserved.
doi:10.1016/j.cplett.2006.05.044

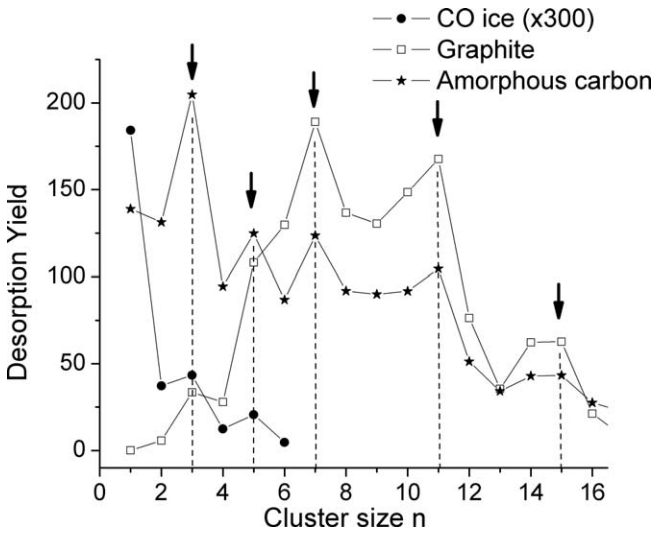

Fig. 1. Desorption yields for the C_n^+ ion clusters produced by ^{252}Cf FF impact on CO ice, laser vaporization/ionization of an amorphous and graphite carbon target. Arrows indicate the magic numbers.

2. Experimental methods

The experimental details of the ^{252}Cf-PDMS-TOF technique can be found elsewhere [25–27]. Briefly, a CO ice target was grown by condensation of CO gas over an Au film at a controlled low temperature (~25 K). Fission fragments from a ^{252}Cf source impact onto the CO ice target inducing desorption of positive and negative ions, as well as neutral particles, at high vacuum conditions (10^{-9} mbar) [27]. The desorbed ions are accelerated by an extraction field towards the drift region and detected by the stop detector. In Fig. 1, the C_n^+ desorption yield is depicted.

The UV laser vaporization/ionization analysis were performed in the linear mode of a BRUKER/BIFLEX III mass spectrometer, equipped with a 337 nm UV nitrogen laser (3 ns FWHM, 200 μJ mean energy per pulse) from Laser Science Inc. A photodiode detects the laser pulse and generates the start signal for the TOF measurement. The C_n^+ desorption yields of the laser vaporization/ionization of the amorphous carbon (made by electron-sputtering deposition from a graphite carbon rod) and of graphite (graphite carbon rods were purchased from Le Carbone-Lorraine, France) targets are also presented in Fig. 1.

3. Computational details

Positively charged carbon cluster structures were calculated using DFT at the B3LYP/6-311 G** level, with the JAGUAR 6.0 software [28]. The basis set superposition error (BSSE) was found to be of the order of 0.02 eV. The accuracy of the B3LYP functional is known to be of the order of ~3 kcal/mol, meaning that conformers differing by less than that amount cannot be distinguished at this level of calculation. No symmetry restrictions have been imposed in the process of geometry optimization. A vibrational analysis was performed in order to verify that the optimized structures correspond to real minima in the potential energy surfaces.

4. Results and discussion

A systematic search for all the possible isomers has been performed (Fig. 2) and their total internal energies (including the zero-point correction) are presented in Table 1. The obtained structures can be classified by their conformational similarities or, as proposed below, by their total internal energy. The taxonomic exercise consists in conciliating logically these different types of sorting.

4.1. Deviation plot analysis (D-plot)

Let $E_n(i)$, be the total energy of the ith isomer of the C_n^+ cluster (values in Table 1) and $\overline{E}(n)$ the average energy of all n-isomers. A linear dependence on n is found for this average energy: $\overline{E}(n) = 19.36–1036.7n$. For each isomer, the deviation energy $D_n(i)$ is defined as: $D_n(i) = \overline{E}(n) - E_n(i)$,

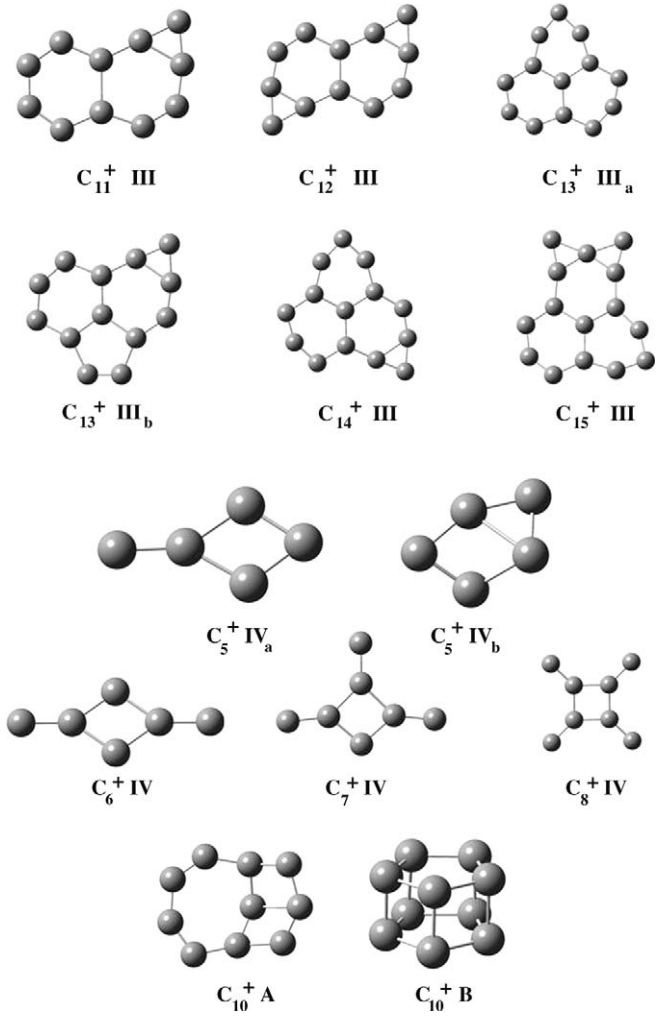

Fig. 2. Optimized geometries of the *Series III* and *IV* clusters at the DFT/B3LYP/6-311G** level of calculation.

Table 1
Carbon cluster internal energy, including ZPE correction, and $D_n(i)$ values at the DFT/B3LYP/6-311G** level of calculation

Cluster	$E_n(i)$ (eV)	$D_n(i)$ (eV)	Cluster	$E_n(i)$ (eV)	$D_n(i)$ (eV)	Cluster	$E_n(i)$ (eV)	$D_n(i)$ (eV)
C^+	−1018.55	–	C_7^+ IV	−7233.20	−4.32	C_{12}^+ I	−12421.71	0.70
C^0	−1028.29	–	C_8^+ II	−8275.61	1.39	C_{12}^+ III	−12419.57	−1.44
C_2^+ I	−2052.92	−1.12	C_8^+ I	−8275.42	1.20	C_{13}^+ II	−13459.45	1.74
C_3^+ II	−3091.94	1.21	C_8^+ IV	−8268.71	−5.51	C_{13}^+ I	−13458.21	0.51
C_4^+ I	−4128.03	0.60	C_9^+ I	−9312.07	1.15	C_{13}^+ III_a	−13456.22	−1.48
C_4^+ II/IV	−4127.79	0.36	C_9^+ II	−9311.59	0.67	C_{13}^+ III_b	−13456.05	−1.65
C_5^+ I	−5165.16	1.03	C_{10}^+ II	−10350.50	2.88	C_{14}^+ II	−14497.61	3.21
C_5^+ IV_a	−5163.60	−0.53	C_{10}^+ I	−10348.63	1.02	C_{14}^+ I	−14494.68	0.28
C_5^+ IV_b	−5163.06	−1.06	C_{10}^+ A	−10344.69	−2.92	C_{14}^+ III	−14492.16	−2.24
C_6^+ I	−6201.96	1.13	C_{10}^+ B	−10343.64	−3.97	C_{15}^+ II	−15534.16	3.06
C_6^+ II	−6201.39	0.56	C_{11}^+ II	−11387.43	3.12	C_{15}^+ I	−15531.14	0.04
C_6^+ IV	−6198.75	−2.08	C_{11}^+ I	−11385.19	0.88	C_{15}^+ III	−15527.69	−3.41
C_7^+ II	−7239.48	1.96	C_{11}^+ III	−11383.91	−0.40	C_{16}^+ II	−16569.46	1.67
C_7^+ I	−7238.77	1.25	C_{12}^+ II	−12422.40	1.39	C_{16}^+ I	−16567.59	−0.20

so that the larger the $D_n(i)$ value, the lower the energy of the isomer and more stable it is. The relevant aspect of the D-plot is that certain isomers have the same systematic deviation, so that they can be gathered into series (Fig. 3).

Some important features become evident in the D-plot for C_n^+: (i) four cluster series can be identified by their D-behavior as represented by the four solid lines in the figure; (ii) the $D_n(i)$ value indicates the relative cluster stability of each species within each series, and (iii) for a given value of n, the D-plot also shows the relative stability of the different isomers.

4.2. Series characteristics

Series I: All members up to $n = 16$ are linear clusters. Remarkable is the fact that the (positively charged) linear trimer structure, previously reported in the literature [24], was not observed at this level of calculation. However, it is worth mentioning that in [24] the linear structure was optimized at the UB3LYP level followed by a single-point calculation at the B3LYP level.

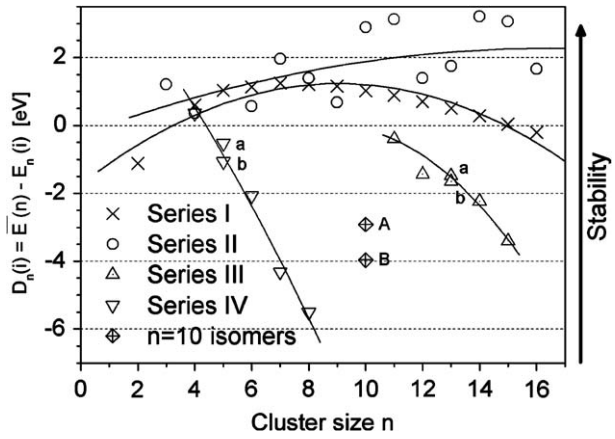

Fig. 3. D-plot: Deviation of the internal cluster energy as a function of the nuclearity n. $D_n(i) = \overline{E}(n) - E_n(i)$, where $\overline{E}(n)$ is the average energy and $E_n(i)$ the cluster energy. Points labeled (a) and (b), for $n = 5$ and 13, correspond to isomers within the respective series. Points labeled (A) and (B), for $n = 10$, correspond to two isomers which do not belong to any of the series.

Series II: This series is characterized by a monocyclic ring structure of carbon atoms. All cyclic structures up to $n = 16$, except for $n = 5$, were obtained at this level of calculation.

Series III: The members of this series present fused ring structures with at least one 6-membered ring, typical of the graphite structure (Fig. 2). The first (C_{11}^+ III) and second (C_{12}^+ III) member of *Series III* are formed by two 6-membered fused rings plus one and two attached carbon atoms, respectively. A third fused ring is formed at $n = 13$ and persists up to $n = 15$ (see C_{13}^+ $III_{a,b}$, C_{14}^+ III and C_{15}^+ III structures).

Series IV: The members of this series are characterized by the existence of the C_4^+ II core structure to which further carbon atoms, up to $n = 8$, are attached (Fig. 2). Larger structures, $n > 9$, have resulted unstable at the level of calculation employed.

Two new isomers for clusters with $n = 10$ were obtained. The C_{10}^+ A isomer presents a complex structure made of two 4-membered and one 7-membered rings fused together. The C_{10}^+ B structure presents two parallel connected 5-membered rings. Similar structures with two 4-membered or two 6-membered parallel rings were not found. The failure to observe any fullerene-like structure for $n < 16$ agrees with the experimental results of Sedo et al. [7].

Series I and *II* structures agree with the previously reported theoretical (for $n = 1$–10) [2,24] and experimental results [13,14]. *Series III* and *IV* structures are difficult to be experimentally identified by ion chromatography [13,14]. Because of the good agreement between the predicted structures and the ones observed experimentally for the smaller cluster, we believe that the four series should probably coexist.

4.3. Mass abundance

The analysis of the experimental data presented in Section 2 is aimed at elucidating the cluster production/ionization using ^{252}Cf fission fragment and 337 nm UV laser pulses as vaporization sources.

In the case of the ^{252}Cf fission fragment, a CO ice target was used to guarantee that all the observed carbon clusters were not pre-formed but are produced during the sputtering process. The exponential decrease of the experimental abundance of the carbon clusters produced by ^{252}Cf FF was also observed for other systems (for instance the H_2O ice [26]) and it seems to be a characteristic of the production/ionization of the ^{252}Cf PDMS technique (later confirmed by the stability analysis).

When nitrogen lasers are employed to ablate amorphous carbon targets, the secondary ion abundances show a roughly decrease as the cluster mass increases (Fig. 1). However, when a graphite target is used, the experimental yields are better described by a Maxwell–Boltzman distribution of clusters centered at $n = 5$. Both spectra show the same magic numbers at $n = 3$, 5, 7, 11 and 15, in agreement with those previously reported [8,9]. Since in both cases the same laser intensity was used, two mechanisms are proposed: the condensation of a high density ionized cloud in vacuum (e.g. for amorphous carbon target) and/or the ejection of large excited molecules into vacuum (e.g. for graphite target).

4.4. Cluster stability

The introduction of a stability function S_n can be helpful in analyzing the cluster abundance variations. The stability function is defined as: $S_n = E_{n-1} + E_{n+1} - 2E_n$, where E_n is the cluster total energy, including the zero-point energy correction.

If the abundance distribution is dominated by evaporative cooling, i.e. by assuming that the final step involves the evaporation of atoms, Bjornholm et al. [29] and Klots et al. [30] have proposed an evaporative ensemble model where the cluster abundance I_n is given by:

$$\ln(I_n/I_{n+1}) = \Delta_2 F(n)/kT, \tag{1}$$

where $\Delta_2 F(n) = 2F(n) - F(n+1) - F(n-1)$ is the second difference of the Helmholtz free energy : $F(n) = E_n - TS$. However since the clusters' internal energies are four orders of magnitude larger than their entropies, the entropic contribution can be neglected and $\Delta_2 F(n) \sim S_n - S_{n-1}$.

An identical distribution is predicted by the quasi-equilibrium model of de Heer et al. [31], according to which the cluster abundances may reflect a quasi-equilibrium distribution, where the cluster abundance I_n is given by:

$$\ln(I_n^2/I_{n+1}I_{n-1}) = \Delta_2 \mathrm{BE}(N)/kT = (S_n - S_{n-1})/kT, \tag{2}$$

with $\Delta_2 \mathrm{BE}(N) = 2E_b(n) - E_b(n+1) - E_b(n-1) = S_n - S_{n-1}$ and where $E_b(n)$ is the binding (or cohesive) energy of the cluster.

The cluster production mechanism and ionization efficiency, either by laser vaporization/ionization or by the sputtering induced by energetic ion impact, can be probed by comparing the experimental intensities (Fig. 4a,b) with the theoretical abundances (Fig. 4c,d) calculated for the

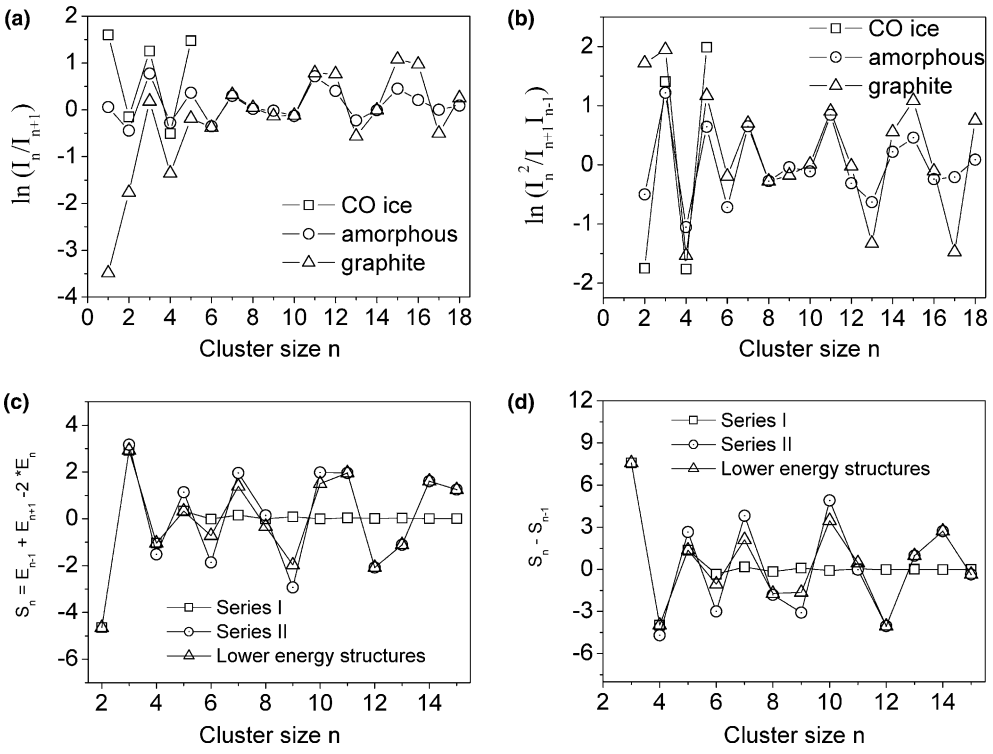

Fig. 4. Experimental cluster abundance distributions (a,b), the stability function S_n (c) and the stabilities predicted by the evaporative and the quasi equilibrium model (d) for *Series I*, *Series II* and for the lower energy structures, as a function of the cluster size n. For $n = 5$, only the member of *Series I* was considered.

members of *Series I, II* and also for the lower energy structures, as a function of the cluster size n. From the comparison of these plots some interesting conclusions can be extracted:

- The carbon clusters produced by ^{252}Cf FF present the same abundance fluctuations as those observed for the stability of *Series I* clusters, differently from all other series. The odd/even periodicity is quite evident with the odd clusters showing larger abundances (Fig. 4a,b). Since the stability analysis describes well the oscillations in the mass spectra (Fig. 4c,d), the exponential decrease must be directly related to the production and/or the ionization mechanism.
- In the range of small carbon clusters (Fig. 4), $n < 6$, data from the amorphous target show a distinct abundance distribution when compared to that of the graphite sample. *Series I* members show a greater abundance when the amorphous target is used. As the linear series describes well both the laser vaporization/ionization of an amorphous carbon target and the ^{252}Cf fission fragments from a CO target, it is concluded that the linear clusters are preferably formed at higher energies, since they do not preserve the memory of the target structure. This result agrees with experimental studies of laser ablation of a graphite target with Nd-YAG laser, where a predominance of odd-numbered carbon clusters was observed [8] at high laser intensities.
- The carbon clusters produced by laser vaporization/ionization have $n = 3$, 5, 7, 11 and 15 as magic numbers, independently of whether the target was graphite or amorphous carbon (Fig. 4a,b). Such numbers are in agreement with those corresponding to fluctuations on the stability function for the low energy isomers (members of the *series I* and *II* only), except for $n = 15$ (Fig. 4c,d). The contribution of *Series IV* is not observed and, for $n > 12$ higher energy isomers (*Series III*) seem to be preferentially formed explaining the magic number at $n = 15$.
- The series fluctuations are better reproduced by the stability function, S_n, (Fig. 4c) rather than the evaporation and quasi–thermal equilibrium model (Fig. 4d). The magic number at $n = 11$ is only reproduced by the stability S_n function (Fig. 4a–c).
- For the laser vaporization/ionization, the production and/or the ionization mechanism seems to play a minor role in the desorption process. Since the amount of evaporated material in laser desorption is much larger than that produced in the ^{252}Cf FF desorption, the quasi-thermal equilibrium expansion process dominates the desorption process. The assumption of a quasi-thermal evolution of the laser-generated plasma in vacuum has been previously reported [32,33].

5. Conclusions

Four series of carbon clusters for $n = 2$–16 are identified in the systematical search performed at the DFT/B3LYP/6-311G** level. Besides the new linear and monocyclic clusters series ($n > 10$), two new series are described: the bi-cyclic and/or tri-cyclic and the rhombic core series. A new methodology to classify the different clusters structures based on the variation of C_n^+ isomers internal energy, rather than their structure, is proposed. The characterization of the series by the D-plot appears to be a more adequate taxonomic methodology to analyze the cluster formation mechanism. A detailed analysis shows that the D values correlate with the cluster abundance, i.e., with the magic numbers observed in the experimental mass spectra. Two competing mechanism of laser production/ionization are proposed: (i) the condensation of a high density ionized cloud in vacuum (e.g. for amorphous carbon target); and (ii) the ejection of excited large molecules into the vacuum (e.g. for graphite target).

The behavior of carbon cluster yields produced by ^{252}Cf fission fragments is similar to that of the fluctuations calculated for the linear series. It is concluded that the linear clusters are preferably formed at higher energies, since they do not depend on the target structure. Characteristics of the target structure and of the desorption mechanism are identified from the analysis of the mass spectra using the stability function. The magic numbers at $n = 3$, 5, 7 and 11, independently of whether the target used is graphite or amorphous carbon, are well described by the fluctuations on the stability analysis, for the lower energy isomers (*Series I* and *II*). For $n > 12$, the stability analysis using the lower energy isomers does not reproduce the abundance fluctuations, showing that higher energy isomers seem to be preferentially formed (e.g. $n = 15$).

Acknowledgements

The authors acknowledge the Brazilian Agencies CNPq, Faperj and CLAF for their support.

References

[1] W. Weltner Jr., R. Van Zee, J. Chem. Rev. 89 (1989) 1713.
[2] A. Van Orden, R.J. Saykally, Chem. Rev. 98 (1998) 2313.
[3] C. Lifshitz, Int. J. Mass Spect. 200 (2000) 423.
[4] E.A. Rohlfing, D.M. Cox, A. Kaldor, J. Chem. Phys. 81 (1984) 3322.
[5] W.R. Creasy, J.T. Brenna, J. Chem. Phys. 92 (1990) 2269.
[6] Y. Zhang, S. Iijima, Appl. Phys. Lett. 75 (1999) 3087.
[7] O. Sedo, M. Alberti, J. Janca, J. Havel, Carbon 44 (2006) 840.
[8] Y.K. Choi, H.S. Im, K.W. Jung, Int. J. Mass Spectrom. 189 (1999) 115.
[9] J.J. Gaumet, A. Wakisaka, Y. Shimizu, Y. Tamori, J. Chem. Soc. Faraday Trans. 89 (1993) 1667.
[10] H. Feld, R. Zurmuhlen, A. Leute, A. Benninghoven, J. Phys. Chem. 94 (1990) 4595.
[11] G. Brinkmalm, P. Demirev, D. Fenyo, P. Hakanson, J. Kopniczky, B.U.R. Sundqvist, Phys. Rev. B 47 (12) (1993) 7560.
[12] C.R. Ponciano, R. Martinez, L.S. Farenzena, P. Iza, M.G.P. Homem, A. Naves de Brito, E.F. da Silveira, K. Wien, Int. J. Mass Spectrom. 17 (2006) 1120.
[13] G. von Helden, M.T. Hsu, P.R. Kemper, M.T. Bowers, J. Chem. Phys. 95 (1991) 3835.

[14] G. von Helden, N.G. Gotts, W.E. Palke, M.T. Bowers, Int. J. Mass Spectrom. Ion Processes 138 (1994) 33.
[15] B.R. Eggen, R.L. Johnson, J.N. Murrell, J. Chem. Soc. Faraday Trans. 90 (1994) 3029.
[16] K.S. Pitzer, E. Clementi, J. Am. Chem. Soc. 81 (1959) 4477.
[17] J.M.L. Martin, P.R. Taylor, J. Phys. Chem. 100 (1996) 6047.
[18] J.M.L. Martin, P.R. Taylor, J. Chem. Phys. 102 (1995) 8270.
[19] J.M.L. Martin, J. El-Jazal, J.P. Francois, Chem. Phys. Lett. 242 (1995) 570.
[20] J.F. Fuller, J. Szczepanski, M. Vala, Chem. Phys. Lett. 323 (2000) 86.
[21] A.F. Jalbout, S. Fernandez, H. Chen, J. Mol. Struct. (Theochem) 584 (2002) 143.
[22] A.F. Jalbout, S. Fernandez, J. Mol. Struct. (Theochem) 584 (2002) 169.
[23] Z. Cao, M. Muhlhauser, M. Hanrath, S.D. Peyerimhoff, Chem. Phys. Lett. 351 (2002) 327.
[24] A. Fura, F. Turecek, F.W. McLaffertty, Int. J. Mass Spectrom. 217 (2002) 81.
[25] R.D. Macfarlane, in: A.C.A. Souza, E.F. da Silveira, J.C. Nogueira, M.A.C. Nascimento, D.P. Almeida (Eds.), Collision Processes of Ion, Positron, Electron and Photon Beams with Matter, World Scientific, Singapore, 1991.
[26] V.M. Collado, L.S. Farenzena, C.R. Ponciano, E.F. da Silveira, K. Wien, Surf. Sci. 569 (2004) 149.
[27] L.S. Farenzena, R. Martinez, P. Iza, C.R. Ponciano, M.G.P. Homem, A. Naves de Brito, E.F. da Silveira, K. Wien, Int. J. Mass Spectrom. 251 (2006) 1.
[28] Jaguar 5.5 and Jaguar 6.0, Schroedinger Inc. Portland, OR, 2004.
[29] S. Bjornholm, J. Borggreen, O. Echt, K. Hansen, J. Pedersen, H.D. Rasmussen, Z. Phys. D 19 (1991) 47.
[30] C.E. Klots, J. Chem. Phys. 92 (21) (1988) 5864.
[31] W.A. de Heer, W.D. Knight, M.Y. Chou, M.L. Cohen, in: H. Ehrenreich, D. Turnbull (Eds.), Solid State Physics, vol. 40, Academic, New York, 1987, p. 93.
[32] F.A. Fernández-Lima, V.M. Collado, C.R. Ponciano, L.S. Farenzena, E. Pedrero, E.F. da Silveira, Appl. Surf. Sci. 217 (2003) 202.
[33] V.M. Collado, F.A. Fernández-Lima, C.R. Ponciano, M.A. Chaer-Nascimento, E.F. da Silveira, Phys. Chem. Chem. Phys. 7 (2005) 1971.